International Journal of Multiphase Flow 36 (2010) 261–272

Contents lists available at ScienceDirect

International Journal of Multiphase Flow

journal homepage: www.elsevier.com/locate/ijmulflow

A moment method for splashing and evaporation processes of polydisperse sprays

Lukas Schneider [a,*], Nechtan Le Lostec [b], Philippe Villedieu [b], Amsini Sadiki [a]

[a] TU Darmstadt, EKT, Petersenstrasse 30, 64287 Darmstadt, Germany
[b] ONERA, 2 Avenue Edouard-Belin, 31055 Toulouse, France

ARTICLE INFO

Article history:
Received 27 November 2008
Received in revised form 4 December 2009
Accepted 6 December 2009
Available online 16 December 2009

Keywords:
Polydisperse spray
Particle trajectory crossing
Sectional method
Quadrature method of moments
Splashing

ABSTRACT

A new moment method for the modelling of polydisperse sprays is proposed that simultaneously takes into account the dispersion in droplet size and droplet velocity. For the derivation of this Eulerian method the kinetic spray equation is used which constitutes a partial differential equation for the probability density function of droplets. To reduce the complex kinetic spray equation to a form that can be managed with the available numerical procedures, moment transforms with respect to the droplet velocity and the droplet size are conducted. The resulting moment equations are closed by choosing an approximate probability density function which applies to polydisperse sprays. The method is successfully tested for configurations in which a polydisperse spray is either splashed, evaporated or effected by a Stokes drag force. The tests are organised in such a way that crossing of two spray distributions is always included. The new method is able to capture the polydisperse nature of sprays as well as the bi-(or multi-) modal character of the droplet velocity distribution function, for example, when droplets cross each other.

1. Introduction

It is widely accepted that there is an urgent demand to limit pollutant emissions and reduce fuel consumption in the combustion of carbon fuels. One step to achieve these objectives is the optimisation of existing combustion technologies, the most common being direct injecting diesel, spark ignition and aeroplane engines. In these the liquid fuel is injected into the combustion chamber where it atomises and forms a spray that evaporates. The behaviour of the spray has a strong influence on the mixing process between oxidiser and fuel, which determines the ignition and burning processes that follow. Still, these complex processes and their interactions are not completely understood (cf. Merker et al., 2006). In addition, correlations between combustion engine tuning parameters needed for engine design can only be predicted with expensive and time-consuming experiments. Only recently, with the extensive use of computer resources, has the development of new and efficient combustion technologies been accelerated using methodologies of computational fluid dynamics (CFD) (cf. Boileau et al., 2008). These methodologies are not mature, i.e. there is still room for improvement in speed, reliability and accuracy, particularly for the prediction of the highly unsteady spray behaviour in combustion chambers. The description of the unsteady fuel spray in combustion engines is either computationally very expensive or too complex for the existing CFD-tools (cf. Ham et al., 2003; Riber et al., 2009; and Desjardins et al., 2008; Fox, 2008, respectively). One example is the lean combustion technology in new aeroplane engines which reduces the NO_x emission. Combustion instabilities are more likely to occur in this technology and hence, steady RANS simulations have to be replaced by unsteady LES calculations in order to predict the behaviour of the reactive, two-phase flow system. This challenging task will be the subject of intensive research for years to come.

The two main approaches classically used to describe the gas-spray behaviour are the Euler–Lagrange and the Euler–Euler method. The spray part of these methods is summarised and briefly discussed.

The Lagrangian procedure (cf. Rueger et al., 2000; Crowe et al., 1998; O'Rourke, 1981; Dukowicz, 1980), also called the particle stochastic method, treats the kinetic spray equation by solving the motion of a large number of numerical particles (parcels) in a space equipped with variables of time, position and droplet velocity, size and temperature or other relevant quantities. The mean spray properties, e.g. for the droplet velocity and mass transfer, at position $\mathbf{x}$ and time t, which are needed for the coupling with the gas phase, are obtained by averaging over a representative sample of parcels that cross a defined volume around $\mathbf{x}$ within a certain time interval including t.

The choice of the sample size is a trade off between spatial and temporal resolution, computational costs and accuracy of the solution. Lagrange computation with small sample volumes and short time intervals with a large number of parcels allow the detailed prediction of an unsteady, polydisperse spray flow. However, the computational costs increase with the number of parcels.

* Corresponding author. Tel.: +49 (0)6151 16 2533; fax: +49 (0)6151 16 6555.
E-mail addresses: schneider@ekt.tu-darmstadt.de (L. Schneider), Nechtan.Le_Lostec@onera.fr (N. Le Lostec), Philippe.Villedieu@onera.fr (P. Villedieu), sadiki@ekt.tu-darmstadt.de (A. Sadiki).

0301-9322/$ - see front matter © 2009 Elsevier Ltd. All rights reserved.
doi:10.1016/j.ijmultiphaseflow.2009.12.003

Another problematic issue in the simulation of unsteady spray flows with Euler–Lagrange methods is the choice of the injection frequency of new numerical particles. One has to make sure that the numerical results do not depend on this parameter.

It was observed by Riber et al. (2009) that the speedup of the Euler–Lagrange method with increasing number of processors is not perfect and it strongly depends on the type of computational grid (hexahedron-based or tetrahedron-based). They show that the drop of performance is not due to large communication costs but originate from the parallel load imbalance generated by the partitioning algorithm. Riber et al. (2009) use the unsteady test configuration of Borée et al. (2001) to compare their Euler–Lagrange computations to experimental measurements for moderate mass loadings. They report that the overall CPU and memory requirements for high-accuracy computations of the particle phase is less than the large eddy (LES) gas computations, indicating that with larger mass loadings the computational costs increase.

By describing the dispersed phase with an Eulerian method, balance equations for various density fields of physical droplet quantities are solved at each position and time (cf. Février et al., 2005; Drew and Passman, 1999; Passman et al., 1984). This procedure has the advantage that, irrespective of the amount of droplets in a region, the same number of equations always have to be solved; hence in Euler–Euler computations a cost is added for the dispersed phase which is independent of the mass loading. Moreover, the solver of both phases can be parallelised with the same strategy (cf. Riber et al., 2009). In consideration of these issues, it is expected and also shown by Riber et al. (2009) that the speedup of the particle phase computation behaves equally well as the speedup of the gas phase computation.

From the above properties of Euler–Lagrange and Euler–Euler methods it is expected that Euler–Euler methods could be a good alternative for spray LES computations, in particular for computations for dense and unsteady particle flows using massively parallelised computers. Of course, this body of research can only be a first stage in the development of a new Euler–Euler method. That is why it is too early to compare the computational costs of the proposed method to other more advanced approaches, in particular because the test cases considered in this paper are too academic. Advantages of such an approach can only be examined in large 3D unsteady computations. In a first stage the new method has to be assessed in simpler configurations, as is done in this paper.

The Eulerian description of dispersed particles has certain principle limitations. By using a two fluid model (cf. Février et al., 2005; Kaufmann, 2004; Groll, 2002), for example, the polydisperse character of the spray can only be captured in a very crude manner, because only two superposed and coupled sets of Navier–Stokes-like equations for the gas and the droplet phase are considered. The shape of the droplet distribution has to be presumed beforehand, which excludes the description of coalescence and breakup. There are several Eulerian approaches available in the literature for the consideration of the polydisperse character using a kinetic spray equation. These are the methods of moments (cf. Grosch et al., 2007), the class or sectional methods (cf. Vanni, 2000; Sirignano, 1999), the methods of characteristics (cf. Rhee et al., 2001), the methods of weighted residual (cf. Costa et al., 2006) and the method of Laplace transforms (cf. Ghosal and Herrmann, 2006), to mention the most common approaches. Here, a method is used which was developed by Gelbard et al. (1980), Domelevo (2001), Laurent and Massot (2001), Laurent et al. (2004), and Dufour and Villedieu (2005). In this approach, hereafter called sectional method, the size space is discretised into fixed intervals, in which balance equations for lower order moments in size for each interval are solved. This treatment of the kinetic spray equation allows for the accurate prediction of evaporation, drag, breakage and coalescence of sprays. There is a variety of other approaches which are based on the discretisation of the size space. For an overview and a detailed comparison of these methods (including the sectional method) the reader is referred to Vanni (2000) and Grosch et al. (2007).

The sectional method as well as all other Eulerian methods that were developed to treat the spray in size space are not capable of describing the dispersion of droplet velocities at one location. However, this is necessary to capture the crossing of two dilute sprays arising in turbulent spray flows, for example. Recently, Desjardins et al. (2008) (see also Fox, 2008) proposed a quadrature-based moment method (cf. Marchisio and Fox, 2005; Fox et al., 2008, for quadrature methods) that overcomes this drawback by solving balance equations not only for the number, mass and momentum densities but also for the kinetic energy and other higher order moments of the (droplet) number density function (NDF). This method is able to describe the crossing of sprays but it does not take into account the polydisperse character of sprays.

A combination of the sectional method developed by Dufour and Villedieu (2005) and the quadrature method of Desjardins et al. (2008) is the subject of this paper. The objective is to merge both procedures in a way that allows the resulting method to describe the polydisperse nature of sprays as well as the coexistence of two or more droplet velocities at one location. To this end, a new and more general approximate NDF is proposed that reduces to the approximation of Dufour and Villedieu (2005) and Desjardins et al. (2008) if special sets of parameters are chosen.

The paper is organised in the following way. After introducing the kinetic description of polydisperse sprays in Section 2, moment transport equations are derived for fixed intervals in size space (Section 3). In Section 4 the idea of Desjardins et al. (2008) is followed and combined with the propositions of Dufour and Villedieu (2005). It is shown that the parameters of the new approximate NDF are uniquely determined by the chosen moments of the exact NDF, a necessary condition for the accuracy of this method. Section 5 is devoted to the numerical procedures that are applied to solve the moment transport equations. These are the Strang splitting in time and the transport schemes in real and size space. In Section 6 the new method is compared to 'reference' Lagrangian calculations to appraise its capabilities. Three cases are tested. The method is applied first to a configuration where droplets are reflected on a wall but break and lose mass and momentum (called splashing). Secondly, the method is tested in a one-dimensional setting of two crossing spray distributions that evaporate according to a d^2-law. In a third test case two sprays cross each other but are affected by a Stokes drag force. Conclusions are drawn in Section 7.

2. Kinetic description of polydisperse sprays

Similar to the description of molecules in the kinetic gas theory (cf. Boltzmann, 1898; Cercignani, 1988), Williams (1958) proposed the following type of equation to model the behaviour of spray systems,

$$\underbrace{\frac{\partial f}{\partial t}+\nabla_{\mathbf{x}}\cdot(\mathbf{v}f)}_{\text{(I)}}+\underbrace{\nabla_{\mathbf{v}}\cdot(\mathbf{F}f)}_{\text{(II)}}+\underbrace{\nabla_s(\mathrm{K}f)}_{\text{(III)}}+\underbrace{\nabla_\theta(\mathrm{R}f)}_{\text{(IV)}}=\Gamma(f)+\Theta(f). \tag{1}$$

In this equation, f is a function of time t, space $\mathbf{x}$, droplet velocity $\mathbf{v}$, a scalar that characterises the droplet size s and the droplet temperature θ. It is physically interpreted as number of droplets per infinitesimal volume $[x,x+dx]\times[v,v+dv]\times[s,s+ds]\times[\theta,\theta+d\theta]$ and is therefore called number density function (NDF). In (1), (I) represents the free transport of a droplet with velocity $\mathbf{v}$, (II) includes the net force $\mathbf{F}$ that affects a droplet, (III) accounts for the continuous change of the droplet size and (IV) reflects the temperature change of a droplet. Γ and Θ allow for the consideration of discontinuous

interactions between the droplets, i.e. the breakage of one droplet into several others or inversely their collision and coalescence. The quantities $\mathbf{F}$, K and R take into account the interaction with the gaseous phase and have to be modelled. Here, the focus is not on the thermodynamic behaviour of the droplets, but rather on the robustness of the new method, introduced in Sections 4 and 5, under the influence of splashing, evaporation, drag and crossing of dilute spray distributions. Therefore, the dependence of f on θ is omitted and the effects of droplet collision and coalescence assumed to be absent, i.e. R, Γ and Θ are set to zero. In addition, only forces on the droplets of the type

$$\mathbf{F} = \frac{\mathbf{U}_g(t,\mathbf{x}) - \mathbf{v}}{\tau_d(s,\mathbf{v})}, \tag{2}$$

which excludes gravity, buoyancy and other, more subtle forces are considered. The above drag force model (2) includes the velocity difference between a droplet and the gas, $(\mathbf{U}_g - \mathbf{v})$, and the relaxation time of the droplets in the surrounding gas, τ_d. The latter quantity can generally be modelled by the Stokes law (cf. Crowe et al., 1998) or laws for more elevated droplet Reynolds numbers (cf. Putnam, 1961).

In this work the evaporation is modelled by a simple d^2-law and the size variable s is identified with the surface area of a droplet. The d^2-law allows K to be constant. It also implies that the non-symmetric effect of the evaporation which results from the velocity difference between droplets and gas is not taken into account (cf. Abramzon and Sirignano, 1989).

These models and the assumptions that go with them are chosen for clarity reasons. If these assumptions are softened or dropped by using more complex models the moment method, introduced below, remains valid as long as Eq. (1) is the basis of these models and no history terms are taken into account (cf. Laurent and Massot, 2001; Laurent et al., 2004).

In the remainder of this paper the following one-dimensional version of Eq. (1) is dealt with,

$$\frac{\partial(f(t,x,s,v))}{\partial t} + \frac{\partial(vf(t,x,s,v))}{\partial x} + \frac{\partial}{\partial v}\left(\frac{U_g(t,x) - v}{\mathrm{St}(s,v)} f\right) - \mathrm{Ev}\frac{\partial(f(t,x,s,v))}{\partial s} = 0, \tag{3}$$

in which all quantities are disposed of their units. For the definition of the Stokes number, $\mathrm{St}(s,v) := \tau_d/\tau_g$ and the evaporation number $\mathrm{Ev} := \tau_g/\tau_{evap}$ the characteristic time scales for the gas flow, τ_g and for the evaporation, $\tau_{evap} = -S^*/K$ are used. The characteristic surface area S^* and the time scale τ_g have to be adapted to the specific spray problem. In the setting of Eq. (3), S^* may be chosen as the surface of the largest initial droplet. The choice of the time scale, τ_g, depends on the properties of the gas flow. For a turbulent flow, a characteristic integral time scale can be selected, whereas in a laminar flow the ratio of a characteristic length and velocity scale may be appropriate.

The extension of the moment method, presented in this paper, to higher dimensions requires some more considerations. The sectional method as well as the quadrature-based moment method were already extended to two dimensions by Dufour and Villedieu (2005) and Desjardins et al. (2008), respectively. However, the combination of the two methods in two dimensions is subject of current research.

3. Moment transport equations

For the reduced model, the NDF, f, has, apart from its dependencies on x and t, two degrees of freedom, i.e. the surface variable, s, and the velocity variable, v. The only equation that can be used to find an expression for $f(t,x,s,v)$ is the reduced spray Eq. (3). In this work, the aim is not to solve for the NDF explicitly but only for certain moments of it. Therefore, the number of free variables is reduced by performing two moment transforms of Eq. (3) with respect to the velocity and surface space.

The transform with respect to the velocity space leads to equations for a set of velocity moments that are defined according to

$$M_L(t,x,s) := \int_{\mathbb{R}} v^L f(t,x,s,v)\,dv. \tag{4}$$

There is no restriction on the choice of moments but, as will be pointed out below, the set

$$\mathscr{U} := \{M_0, M_1, M_2, M_3\} \in \mathbb{R}^4 \tag{5}$$

allows for a convincing physical interpretation. The moment transform consists of two mathematical operations that are applied consecutively to the spray Eq. (3). First, (3) is multiplied by the respective powers of the velocity variable and then, the emerging equations are integrated over the set $\mathbb{R}$ of all possible velocities. This procedure yields, after some algebra,

$$\begin{aligned}
&\frac{d}{dt}(M_0) - \mathrm{Ev}\frac{\partial}{\partial s}(M_0) = 0,\\
&\frac{d}{dt}(M_1) - \mathrm{Ev}\frac{\partial}{\partial s}(M_1) = \int_{\mathbb{R}} \left(\frac{U_g - v}{St(v,s)}\right) f\,dv,\\
&\frac{d}{dt}(M_2) - \mathrm{Ev}\frac{\partial}{\partial s}(M_2) = 2\int_{\mathbb{R}} \left(v\frac{U_g - v}{St(v,s)}\right) f\,dv,\\
&\frac{d}{dt}(M_3) - \mathrm{Ev}\frac{\partial}{\partial s}(M_3) = 3\int_{\mathbb{R}} \left(v^2\frac{U_g - v}{St(v,s)}\right) f\,dv,
\end{aligned} \tag{6}$$

where the *material time derivative* (cf. Hutter and Jöhnk, 2004)

$$\frac{d(M_L)}{dt} := \frac{\partial}{\partial t}(M_L) + \frac{\partial}{\partial x}(M_{L+1}) \tag{7}$$

is introduced. For the derivation of the integrals on the right-hand side (RHS) of system (6) it is assumed that in velocity space the NDF declines rapidly to zero for large velocity values (e.g. $o(|v|^{-3})$). In physical spray systems this assumption is always satisfied. It is also of interest that

(i) system (6) is unclosed because an expression for the fourth moment in $(6)_4$ is missing (see also (7)),
(ii) the integrals on the RHS of system (6) cannot be evaluated unless a special form for St is considered or the generality of f is reduced,
(iii) $U_g(t,x)$ is assumed to be supplied by some analytical or numerical solution of the gas flow and
(iv) if it were somehow possible to close the above system and evaluate the RHS one would still be confronted with a partial differential equation (PDE) system that exhibits three degrees of freedom. This problem cannot be treated with the numerical methods that are commonly used to solve balance equations in which all fields are functions of space and time only.

To transform Eq. (6) into the usual form of balance equations another moment transform with respect to the surface variable, s, has to be performed. Similar to Laurent and Massot (2001), Laurent et al. (2004) and Dufour and Villedieu (2005), the surface space [0,1] is split into N fixed intervals, $I_k = [s_k, s_{k+1}[\in [0,1]$, $k = 1,\ldots N$, called sections, which constitute the domains of integration.[1] Every interval is equipped with the set of moments,

[1] Applying the moment transform in surface space in the described way, a transport scheme in surface space is derived which is similar to the finite volume scheme in real space (t,x) (Section 5).

$$\mathscr{V}_k := \left\{ M^{(k)}_{0,0}, M^{(k)}_{3/2,0}, M^{(k)}_{3/2,1}, M^{(k)}_{3/2,2}, M^{(k)}_{3/2,3} \right\} \in \mathbb{R}^5, \tag{8}$$

in which the moments are defined according to

$$M^{(k)}_{K,L}(t,x) := \int_{s_k}^{s_{k+1}} s^K \int_{\mathbb{R}} v^L f(t,x,s,v)\, dv\, ds. \tag{9}$$

It has to be admitted that sets other than (8) are admissible, but the first four moments in set $\mathscr{V}_k$ are the only ones that can be physically interpreted as normalised number, mass, momentum and kinetic energy of droplets in section I_k. The last moment in $\mathscr{V}_k$ could be related to the skewness of the NDF in velocity space (cf. Pope, 2000) but as it is not a standardised moment it is simple called mixed moment of order 3 in velocity space and order 3/2 in surface space.

The above moment transform of system (6) yields $5N$ balance equations. They have the form

$$\begin{aligned}
&\frac{d}{dt}\left(M^{(k)}_{0,0}\right) - \mathrm{Ev}\int_{s_k}^{s_{k+1}} \int_{\mathbb{R}} \frac{\partial f}{\partial s}\, dv\, ds = 0,\\
&\frac{d}{dt}\left(M^{(k)}_{3/2,0}\right) - \mathrm{Ev}\int_{s_k}^{s_{k+1}} \int_{\mathbb{R}} s^{3/2}\frac{\partial f}{\partial s}\, dv\, ds = 0,\\
&\frac{d}{dt}\left(M^{(k)}_{3/2,1}\right) - \mathrm{Ev}\int_{s_k}^{s_{k+1}} \int_{\mathbb{R}} s^{3/2} v\frac{\partial f}{\partial s}\, dv\, ds = \int_{s_k}^{s_{k+1}} s^{3/2}\int_{\mathbb{R}} \left(\frac{U_g - v}{St(v,s)}\right) f\, dv\, ds,\\
&\frac{d}{dt}\left(M^{(k)}_{3/2,2}\right) - \mathrm{Ev}\int_{s_k}^{s_{k+1}} \int_{\mathbb{R}} s^{3/2} v^2\frac{\partial f}{\partial s}\, dv\, ds = 2\int_{s_k}^{s_{k+1}} s^{3/2}\int_{\mathbb{R}} \left(v\frac{U_g - v}{St(v,s)}\right) f\, dv\, ds,\\
&\frac{d}{dt}\left(M^{(k)}_{3/2,3}\right) - \mathrm{Ev}\int_{s_k}^{s_{k+1}} \int_{\mathbb{R}} s^{3/2} v^3\frac{\partial f}{\partial s}\, dv\, ds = 3\int_{s_k}^{s_{k+1}} s^{3/2}\int_{\mathbb{R}} \left(v^2\frac{U_g - v}{St(v,s)}\right) f\, dv\, ds,
\end{aligned} \tag{10}$$

in each section I_k with $k = 1, \ldots N$.

The number of free variables is reduced (remark (iv)) but for system (10) the issues in remarks (i) and (ii) remain unsolved.

4. Moment closure

For the closure of PDE-system (10) it is misleading to use the Maxwellian principles of the kinetic gas theory, because, in contrast to the motion of a dilute gas, a dilute spray does not satisfy the conditions of kinetic equilibrium. Nevertheless, it is worthwhile to use Maxwell's idea of approximating the probability density function for the gas molecules using an algebraic function that is physically motivated. In this way the NDF is approximated by

$$\tilde{f}(t,x,s,v) = \sum_{k=1}^{N}\sum_{i=1}^{I} \mathbf{1}_{s_k \leqslant s < s_{k+1}} a^i_k(t,x)\exp(-b_k(t,x)s)\delta_{v-U^i_k(t,x)}, \tag{11}$$

with

$$\mathbf{1}_{s_k \leqslant s < s_{k+1}} = \begin{cases} 1 & \text{if} \quad s_k \leqslant s \leqslant s_{k+1}, \\ 0 & \text{otherwise.} \end{cases} \tag{12}$$

The set

$$\mathscr{W}_k = \left[b_k, a^1_k, \ldots, a^I_k, U^1_k, \ldots, U^I_k \right], \quad k = 1, \ldots, N \tag{13}$$

of $(2I+1)N$ free parameters will later be related to the moments in set $\mathscr{V}_k$. Thereby a specific physical meaning will be given to them. The function $\tilde{f}$ does not contradict the polydisperse character of sprays, nor does it undermine the dispersion of droplet velocities at one location. The method following from (11) may be regarded as a generalisation of the sectional method introduced by Gelbard et al. (1980), Domelevo (2001), Laurent and Massot (2001) and Laurent et al. (2004) – or more precisely its variant proposed by Dufour and Villedieu (2005) – and the quadrature method recently introduced by Desjardins et al. (2008). In the case of $I = 1, N > 1$ the sectional method according to Dufour and Villedieu (2005) is recovered and for $N = 1$, $I > 1$ a method similar to that of Desjardins et al. (2008) is obtained.

The substitution of approximation (11) into the unclosed moment Eq. (10) yields for every section I_k $(k = 1, \ldots N)$

$$\begin{aligned}
&\frac{d}{dt}\left(M^{(k)}_{0,0}\right) - \mathrm{Ev}\int_{s_k}^{s_{k+1}} \int_{\mathbb{R}} \frac{\partial \tilde{f}}{\partial s}\, dv\, ds = 0,\\
&\frac{d}{dt}\left(M^{(k)}_{3/2,0}\right) - \mathrm{Ev}\int_{s_k}^{s_{k+1}} \int_{\mathbb{R}} s^{3/2}\frac{\partial \tilde{f}}{\partial s}\, dv\, ds = 0,\\
&\frac{d}{dt}\left(M^{(k)}_{3/2,1}\right) - \mathrm{Ev}\int_{s_k}^{s_{k+1}} \int_{\mathbb{R}} s^{3/2} v\frac{\partial \tilde{f}}{\partial s}\, dv\, ds\\
&\qquad = \int_{s_k}^{s_{k+1}} s^{3/2}\exp(-b_k s)\sum_{i=1}^{I}\left[a^i_k \frac{U_g - U^i_k}{St(U^i_k, s)}\right] ds,\\
&\frac{d}{dt}\left(M^{(k)}_{3/2,2}\right) - \mathrm{Ev}\int_{s_k}^{s_{k+1}} \int_{\mathbb{R}} s^{3/2} v^2\frac{\partial f}{\partial s}\, dv\, ds\\
&\qquad = 2\int_{s_k}^{s_{k+1}} s^{3/2}\exp(-b_k s)\sum_{i=1}^{I}\left[a^i_k U^i_k \frac{U_g - U^i_k}{St(U^i_k, s)}\right] ds,\\
&\frac{d}{dt}\left(M^{(k)}_{3/2,3}\right) - \mathrm{Ev}\int_{s_k}^{s_{k+1}} \int_{\mathbb{R}} s^{3/2} v^3\frac{\partial f}{\partial s}\, dv\, ds\\
&\qquad = 3\int_{s_k}^{s_{k+1}} s^{3/2}\exp(-b_k s)\sum_{i=1}^{I}\left[a^i_k (U^i_k)^2 \frac{U_g - U^i_k}{St(U^i_k, s)}\right] ds.
\end{aligned} \tag{14}$$

In each section, $\tilde{f}$ is defined by $(1+2I)$ parameters, $\mathscr{W}_k$, that have to be uniquely linked to the set $\mathscr{V}_k$ of moments (see (8)). Otherwise, it cannot be guaranteed that the approximated NDF has the same lower order moments as the exact NDF. In the case of $I = 2$,[2] the relations between the moments in $\mathscr{V}_k$ and the parameters in $\mathscr{W}_k$ are determined by

$$M^{(k)}_{K,L} = \int_{s_k}^{s_{k+1}} s^K \exp(-b_k s)\left\{ a^1_k (U^1_k)^L + a^2_k (U^2_k)^L \right\} ds, \tag{15}$$

for $(K,L) = \{(0,0),(3/2,0),(3/2,1),(3/2,2),(3/2,3)\}$. From these relations it is not obvious that the parameters of $\tilde{f}$ given in $\mathscr{W}_k$ can be uniquely determined by the moments in $\mathscr{V}_k$ because the RHS's of (15) are highly non-linear. The uniqueness and the explicit formulation of the mapping $\mathscr{V}_k \to \mathscr{W}_k$ is subject to the following proposition.

Property 1. *Let $\mathscr{V}_k$ be the set of moments defined in (8) and (9) such that*

$$\begin{aligned}
&\text{(i)}\ M^{(k)}_{0,0} > 0, \quad \text{(ii)}\ M^{(k)}_{3/2,2} \geqslant \frac{\left(M^{(k)}_{3/2,1}\right)^2}{M^{(k)}_{3/2,0}},\\
&\text{(iii)}\ M^{(k)}_{3/2,0} > 0, \quad \text{(iv)}\ \frac{M^{(k)}_{3/2,0}}{M^{(k)}_{0,0}} \in \left]s_k^{3/2}, s_{k+1}^{3/2}\right[,
\end{aligned} \tag{16}$$

then, up to a permutation between subscripts 1 and 2, there exists only one set $\mathscr{W}_k$ of parameters introduced in (11), (13) that satisfies the relations in (15). This solution is given by the inverse function

$$b_k = g_k^{-1}\left(\frac{M^{(k)}_{3/2,0}}{M^{(k)}_{0,0}}\right) \quad \text{with}$$

$$g_k(b) := \begin{cases} \frac{2}{5}\frac{\left(s_{k+1}^{5/2} - s_k^{5/2}\right)}{|I_k|}, & b = 0, \\ \frac{\int_{s_k}^{s_{k+1}} s^{\frac{3}{2}}\exp(-b_k s)ds}{\int_{s_k}^{s_{k+1}}\exp(-b_k s)ds}, & b \neq 0, \end{cases} \tag{17}$$

[2] For values of I larger than 2, the distribution in velocity space can be captured more accurately, i.e. not only bimodal but tri- or multimodal velocity distribution functions can be described. Choosing a larger value for I leads to an extension of the set of moments $\mathscr{V}_k$ and, consequently, the number of equations in system (14) increases.

and the relations

$$
\begin{aligned}
a_k^1 &= (1/2 + x_k)\left(\overline{M}_{3/2,0}^{(k)}\right),\\
a_k^2 &= (1/2 - x_k)\left(\overline{M}_{3/2,0}^{(k)}\right),\\
U_k^1 &= U_k^p - \left(\frac{a_k^2}{a_k^1}\right)^{1/2}\sigma_k^p,\\
U_k^2 &= U_k^p + \left(\frac{a_k^1}{a_k^2}\right)^{1/2}\sigma_k^p,\\
x_k &= \frac{q_k^p/2}{\left((q_k^p)^2 + 4(\sigma_k^p)^6\right)^{1/2}}.
\end{aligned}
\tag{18}
$$

The quantities $\overline{M}_{K,L}^{(k)}$, U_k^p, σ_k^p *and* q_k^p *are defined by*

$$
\begin{aligned}
\overline{M}_{K,L}^{(k)} &= \frac{M_{K,L}^{(k)}}{\int_{s_k}^{s_{k+1}} s_2^3 \exp(-b_k s)ds},\\
U_k^p &= \frac{\overline{M}_{3/2,1}^{(k)}}{\overline{M}_{3/2,0}^{(k)}},\\
\sigma_k^p &= \left(\frac{\overline{M}_{3/2,0}^{(k)}\overline{M}_{3/2,2}^{(k)} - \left(\overline{M}_{3/2,1}^{(k)}\right)^2}{\left(\overline{M}_{3/2,0}^{(k)}\right)^2}\right)^{1/2},\\
q_k^p &= \frac{1}{\overline{M}_{3/2,0}^{(k)}}\left(\overline{M}_{3/2,3}^{(k)} - \overline{M}_{3/2,0}^{(k)}(U_k^p)^3 - 3\left(\overline{M}_{3/2,0}^{(k)}\right)(\sigma_k^p)^2 U_k^p\right).
\end{aligned}
\tag{19}
$$

Eqs. (17)–(19) constitute the mapping $\mathscr{V}_k \to \mathscr{W}_k$.

Note that it was proven by Dufour and Villedieu (2005) that $g_k(b)$ (cf. $(17)_2$) is a strictly decreasing function on $\mathbb{R}$ with the properties: $\lim_{b\to-\infty} g_k(b) = s_{k+1}^{3/2}$ and $\lim_{b\to+\infty} g_k(b) = s_k^{3/2}$. Therefore, using (iv) in each section, g_k can be inverted and a unique solution b_k can be found from Eq. (17).

Note also, that with the solution for b_k, (i), (ii) and (iii), Desjardins et al. (2008) provide the proof that, up to a permutation of $(a_k^1, \mathbf{U}_k^1)$ with $(a_k^2, \mathbf{U}_k^2)$, $\mathscr{W}_k$ is uniquely determined by the set $\mathscr{V}_k = \left\{\overline{M}_{0,0}^{(k)}, \overline{M}_{3/2,0}^{(k)}, \overline{M}_{3/2,1}^{(k)}, \overline{M}_{3/2,2}^{(k)}, \overline{M}_{3/2,3}^{(k)}\right\}$ of normalised moments.

The Eqs. (17)–(19) are of importance for the evaluation of the integrals on the RHS of (14) and for the numerical implementation of the derivatives arising in these equations.

The numerical algorithms used to solve equation system (14) are presented in the following section. The associated initial and boundary conditions are specified for the respective test cases in Section 6.

5. Numerical schemes

As mentioned above, the kinetic spray equation in (3) cannot be solved with the standard numerical schemes used for the treatment of flow problems because the NDF is a function of more variables than just position and time. That is why, in the previous sections, Eq. (3) has been transformed to the system of moment Eq. (14) that allow the application of the well-known finite volume method in real space

$$
\frac{N_i^{n+1} - N_i^n}{\Delta t} = \frac{1}{\Delta x}\left[G(N_{i-r}^n, N_{i-r+1}^n, \ldots, N_{i+s}^n) - G(N_{i-r-1}^n, N_{i-r}^n, \ldots, N_{i+s-1}^n)\right].
\tag{20}
$$

and the sectional method (cf. Dufour and Villedieu, 2005) in surface space

$$
\begin{aligned}
\frac{M_k^{n+1} - M_k^n}{\Delta t} = \mathscr{P} + \frac{1}{|I_k|}\Big[&F\left(M_{k-q}^n, M_{k-q+1}^n, \ldots, M_{k+l}^n\right)\\
&- F\left(M_{k-q-1}^n, M_{k-q}^n, \ldots, M_{k+l-1}^n\right)\Big].
\end{aligned}
\tag{21}
$$

In these schemes, N_i^{n+1} is a general moment in cell $Z_i = [x_i, x_{i+1}] \in [0,1]$ at time $t_n + \Delta t$ and M_k^{n+1} is a general moment in section I_k at time $t_n + \Delta t \cdot G(\cdot)$ and $F(\cdot)$ are fluxes through the cell and section boundaries, respectively, and $\mathscr{P}$ represents a source term coming into play in evaporation. The numerical schemes (20) and (21) are conservative because, due to their structure, no piece of M_k or N_i is artificially added or erased during the transport processes in the respective spaces (cf. LeVeque, 1992).

By using two separate schemes for the surface and real space it is tacitly assumed that the transport in surface and real space can be uncoupled. Indeed, there are numerical algorithms available, called fractional step methods in time, that allow (14) to be split into less complex subproblems which then can be treated with different numerical schemes (cf. LeVeque, 1992). In this work, equation system (14) (with $I = 2$) is divided into the subproblems of transport in real space, drag and evaporation. These subproblems are solved in each time step Δt in the following sequence: (i) $\Delta t/2$ transport, (ii) $\Delta t/2$ drag, (iii) Δt evaporation, (iv) $\Delta t/2$ drag, (v) $\Delta t/2$ transport. This sequence is denoted Strang splitting in time, for which it was proven (cf. Strang, 1968; Bobylev and Ohwada, 2001) that the accuracy of the overall method remains second order in all variables if the numerical schemes of each subproblem are second order in the respective variable. For each of the above steps the solution of the previous step is used as 'initial condition' but for the first fractional step (here transport) the solution of the previous time-step, the solution at time t_n or the initial condition of the whole problem is taken into account. The solution of the last step is also the solution of system (14) at time $t_n + \Delta t$.

Transport: The mathematical problem of transport in real space

$$
\begin{aligned}
&\frac{\partial \mathbf{W}^{(k)}}{\partial t} + \frac{\partial \mathbf{H}^{(k)}}{\partial x} = 0\\
&\text{with}\quad \mathbf{H}^{(k)} = \int_{\mathbb{R}} v\mathbf{K}^{(k)} \sum_{j=1}^{2}\left\{a_k^j \delta_{v-U_k^j}\right\} dv
\end{aligned}
\tag{22}
$$

and

$$
\mathbf{W}^{(k)} = \begin{pmatrix} M_{0,0}^{(k)} \\ M_{3/2,0}^{(k)} \\ M_{3/2,1}^{(k)} \\ M_{3/2,2}^{(k)} \\ M_{3/2,3}^{(k)} \end{pmatrix}, \qquad \mathbf{K}^{(k)} = \begin{pmatrix} E_0^{(k)} \\ E_{3/2}^{(k)} \\ E_{3/2}^{(k)} v \\ E_{3/2}^{(k)} v^2 \\ E_{3/2}^{(k)} v^3 \end{pmatrix},
\tag{23}
$$

supplemented by appropriate initial and boundary conditions can be regarded as the extension of the pressureless gas equation studied by Bouchut (1994). It is treated numerically with a finite volume method, as proposed in Eq. (20). The terms $E_M^{(k)}$ in (23) are defined according to

$$
E_M^{(k)} = \int_{s_i}^{s_{i+1}} s^M \exp(-b_k s)ds.
\tag{24}
$$

An equidistant discretisation, $\{x_1, \ldots, x_J\}$, of the real line [0,1] is introduced with $x_1 = 0$ and $x_J = 1$, where one cell, Z_i, has the size $|Z_i| = \Delta x_i = \Delta x$. In the centre of each cell at a fixed time $t_n + \Delta t$, $\mathbf{W}^{(k)}$ is assumed to have the value $\mathbf{W}_i^{n+1}$.[3]

In this work, a first order scheme for the free transport ($r = 0$, $s = 1$ in (20)) is used which leads to the following expression

$$
\frac{\mathbf{W}_i^{n+1} - \mathbf{W}_i^n}{\Delta t} = \frac{1}{\Delta x}\left[G(\mathbf{W}_i^n, \mathbf{W}_{i+1}^n) - G(\mathbf{W}_{i-1}^n, \mathbf{W}_i^n)\right].
\tag{25}
$$

The numerical flux function $G(\cdot)$ is derived from (22)–(24) and reads

[3] In this paragraph, the index (k) is skipped for clarity reasons. In the fractional step of transport the scheme derived here is applied to each section I_k independently.

$$G(\mathbf{W}_i^n, \mathbf{W}_{i+1}^n) = \int_{\mathbb{R}} \frac{1}{2}(v+|v|)\mathbf{K}\sum_{l=1}^{2}(a_l(t_n,x)\delta_{v-U_l(t_n,x)})dv\Big|_i + \int_{\mathbb{R}} \frac{1}{2}(v-|v|)\mathbf{K}\sum_{l=1}^{2}(a_l(t_n,x)\delta_{v-U_l(t_n,x)})dv\Big|_{i+1}, \quad (26)$$

where the operator $(\cdot)|_i$ forces the quantities in brackets to belong to cell Z_i. $G(\mathbf{W}_i^n, \mathbf{W}_{i+1}^n)$ can be interpreted as fluxes of the moments in $\mathbf{W}_i^n$ through the right boundary of cell Z_i. $G(\mathbf{W}_{i-1}^n, \mathbf{W}_i^n)$, on the other hand, are the fluxes through the left boundary of the same cell.

Similar to the proof of Bouchut (1994), it can be shown that the above scheme is of first order. Here, the scheme in (25) and (26) is not proven to preserve the realisability conditions (i) to (iv) in (16) nor is the maximum principle on the velocities addressed. The results in Section 6 are calculated with the CFL condition

$$dt < \frac{dx}{\max_l(U_k^l)}, \quad (27)$$

and no unphysical negative masses or artificial oscillations were observed. Desjardins et al. (2008) proved that condition (27) is sufficient to satisfy the realisability condition for monodisperse sprays (similar to conditions (ii) and (iii) in (16)). For the method presented here, the surface variable is assumed to be fixed during the fractional step of transport in real space, i.e. no transport in surface space is taking place while the fields are transported in real space. Therefore, conditions (i) and (iv) in (16) should remain valid during the transport in real space. The numerical results in Section 6 support this assumption.

It is believed that the scheme in (25) and (26) can be extended to higher orders by approximating the fluxes through the boundaries with higher order interpolations of $\mathbf{W}^n$ at the boundaries rather than simply using the values at the middle of each cell. The realisation of this classical MUSCL extension (cf. LeVeque, 1992) has been postponed for future study.

Evaporation: The derivation of the numerical scheme for the evaporation step commences with the reduced spray equation

$$\frac{\partial}{\partial t}(f) - \mathrm{Ev}\frac{\partial}{\partial s}(f) = 0, \qquad f(t=t_n) = f_n, \quad (28)$$

in which only the evaporation term is retained. In this step, it is assumed that f is not changing with respect to x or v. Eq. (28) is a linear hyperbolic PDE that has the solution $f(s,t) = f_n(s + E_v(t-t_n))$ for all $(s,t) > (0,t_n)$.

The evaporation step can be split into three substeps. First, the parameters in set $\mathscr{W}_k$ are computed from the moments in set $\mathscr{V}_k$ at time t_n with the help of the mapping $\mathscr{V}_k \to \mathscr{W}_k$, as defined in (17)–(19). Then, by simply introducing the solution of (28) into the definition of moments $M_{K,L}^{(k)}$ (see (9)) at time $t_n + \Delta t$, the following expression

$$M_{K,L}^{(k)}(t_n+\Delta t) = \int_{s_k}^{s_{k+1}} s^K \int_{\mathbb{R}} v^L f^n(s + E_v\Delta t)\, dv\, ds \quad (29)$$

is obtained in a section I_k and some fixed cell Z_i. If the exact solution $f_n(s+E_v\Delta t)$ is replaced by its approximation $\tilde{f}_k^n(s+E_v\Delta t)$ and the emerging integrals are rearranged, the following scheme is finally obtained

$$M_{K,L}^{(k)}(t_n+\Delta t) - M_{K,L}^{(k)}(t_n) = +\mathscr{P}1_{K,L}^{(k)}(t_n) + \mathscr{P}2_{K,L}^{(k)}(t_n) + \frac{1}{|I_k|}\left[F(M_{K,L}^{(k)}(t_n), M_{K,L}^{(k+1)}(t_n)) - F(M_{K,L}^{(k-1)}(t_n), M_{K,L}^{(k)}(t_n))\right] \quad (30)$$

for each section I_k and a fixed cell Z_i. The functions arising in (30) are expressed as follows

$$F(M_{K,L}^{(k)}(t_n), M_{K,L}^{(k+1)}(t_n)) = |I_{k+1}| \int_{s_{k+1}}^{s_{k+1}+\mathrm{Ev}\Delta t} u^K \times \int_{\mathbb{R}} v^L \tilde{f}_n^{(k+1)}(u,v)\, dv\, du \quad (31)$$

for the fluxes over the section boundaries and

$$\mathscr{P}1_{K,L}^{(k)}(t_n) = \int_{s_k+\mathrm{Ev}\Delta t}^{s_{k+1}} \left((u-\mathrm{Ev}\Delta t)^K - u^K\right)\int_{\mathbb{R}} \tilde{f}_n^{(k)}(u,v)\, dv\, du$$
$$\mathscr{P}2_{K,L}^{(k)}(t_n) = \int_{s_{k+1}}^{s_{k+1}+\mathrm{Ev}\Delta t} \left((u-\mathrm{Ev}\Delta t)^K - u^K\right)\int_{\mathbb{R}} \tilde{f}_n^{(k+1)}(u,v)\, dv\, du \quad (32)$$

for the source terms of evaporating droplets. It should be noted that in the case of $(K,L) = (0,0)$ the source terms are identical to zero. This agrees with the interpretation that in the region $s =]0,1]$ the number of droplets is not reduced by evaporation. Only at the left boundary of the first section, I_1, droplets vanish and the number of droplets reduces to zero. For the moments other than $(K,L) = (0,0)$ the source terms are in general nonzero. For the case $(K,L) = (3/2,0)$, $\mathscr{P}1_{K,L}^{(k)}$ and $\mathscr{P}2_{K,L}^{(k)}$ are interpreted as loss of mass in section I_k and in case $(K,L) = (3/2,1)$ as loss of momentum. Similar interpretations hold for other moments.

It was proven by Dufour and Villedieu (2005) that the scheme in (30)–(32) is consistent of order 2 in surface space if the sections are of the same size, and of order 1 if they are not equisized. In addition, it was demonstrated by Dufour and Villedieu (2005) that the moments $(K,L) = (0,0)$ and $(K,L) = (3/2,0)$, i.e. the number and mass of droplets in a section, remain bounded and positive for all times $t \in [0,T]$ if the CFL condition $\mathrm{Ev}\Delta t \leqslant |I_k|$ is satisfied. The same condition is used to prove that the maximum principle on the ratio $M_{3/2,0}^{(k)}/M_{0,0}^{(k)}$ is satisfied. The latter property is necessary to ensure condition (iv) in (16). It is assumed that the maximum principle on the velocities is satisfied because in the fractional step of transport in surface space, the velocity variable is fixed, i.e. no transport is taking place in real space.

Drag: In the fractional step of drag, the equation system

$$\begin{aligned}
&\frac{\partial}{\partial t}\left(M_{0,0}^{(k)}\right) = 0, \qquad \frac{\partial}{\partial t}\left(M_{3/2,0}^{(k)}\right) = 0,\\
&\frac{\partial}{\partial t}\left(M_{3/2,1}^{(k)}\right) = \int_{s_k}^{s_{k+1}} \mathsf{E}_k \sum_{i=1}^{I}\left[a_k^i \frac{U_g - U_k^i}{St(U_k^i,s)}\right] ds,\\
&\frac{\partial}{\partial t}\left(M_{3/2,2}^{(k)}\right) = 2\int_{s_k}^{s_{k+1}} \mathsf{E}_k \sum_{i=1}^{I}\left[a_k^i U_k^i \frac{U_g - U_k^i}{St(U_k^i,s)}\right] ds,\\
&\frac{\partial}{\partial t}\left(M_{3/2,3}^{(k)}\right) = 3\int_{s_k}^{s_{k+1}} \mathsf{E}_k \sum_{i=1}^{I}\left[a_k^i (U_k^i)^2 \frac{U_g - U_k^i}{St(U_k^i,s)}\right] ds,
\end{aligned} \quad (33)$$

is taken into account for each of the N sections I_k and for each of the J cells Z_i. Here, E_k is an abbreviation for $s^{3/2}\exp(-b_k s)$. The differential equations in (33) are highly coupled and also show a strong non-linearity behaviour because the parameters on the RHS are related to the moments on the left-hand side via the non-linear mapping $\mathscr{V}_k \to \mathscr{W}_k$. Nonetheless, a second order Runge–Kutta procedure is applied that assumes the RHS to be computed at time t_n or at the previous Runge–Kutta step.

6. Applications and results

To test the ability of the method outlined in Sections 3–5, it was applied to three simplified spray problems that change the spray distribution in surface space, first through splashing,[4] second

[4] This is most likely the first time splashing of a polydisperse spray has been captured by an Eulerian procedure. Desjardins et al. (2008) were able to describe splashing for a monodisperse spray.

through evaporation, and third through a size-dependent Stokes drag force. All test cases were organised in such a way that crossing of two spray distributions was included. Solutions to the same test cases were also computed using a Lagrangian method. They are regarded as accurate reference solutions. The numerical algorithms for the Eulerian method were explained in Section 5. For the Lagrangian method simple implementations of the method presented in Crowe et al. (1998) were used. The models for evaporation, splashing and drag were incorporated into the Lagrangian code without any cut back.

6.1. Test case: splashing of polydisperse spray

When droplets hit a wall, break and rebound with a certain velocity and size, they are said to splash on that wall. So far, it has not been possible to capture this phenomenon with Eulerian methods, because they assume that locally the velocity of a droplet is tied to its size and its position. This assumption does not hold for splashing sprays since, near the wall, neighbouring droplets of the same size may exhibit completely different velocities. The method presented in Sections 3–5 does not rely on this assumption and therefore, as will be demonstrated, it allows the accurate description of splashing sprays.

In this case, a truncated Gaussian spray distribution (see line marked 'inlet' in Fig. 1) enters the domain from the left ($x = 0$) and is freely transported through it. The right boundary ($x = 1$) is modelled as a wall, on which the droplets break, lose mass and momentum. A droplet that is rebound from the wall is assumed to exhibit the velocity

$$V = -\alpha V', \tag{34}$$

the diameter

$$D = \beta D', \tag{35}$$

and the mass

$$M = (1-\gamma)M'. \tag{36}$$

The symbols with a prime represent the respective quantities of the droplet before it hits the wall. The parameters α, β and γ are related to the coefficient of restitution, the partition of a droplet and the loss of fluid mass (through deposition or sudden evaporation) on the wall, respectively.

If the droplets in a spray are assumed to be spherical and of size d, their mass, m, and their number, n, are related by

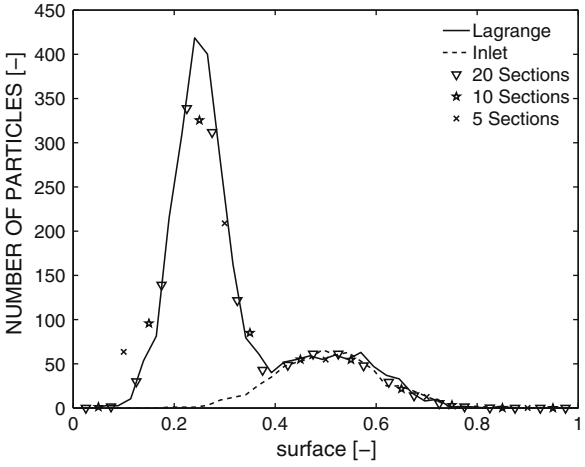

Fig. 1. Droplet distribution at $x = 0.9$; splashing at a wall with parameters $\alpha = 0.9$, $\beta = 0.7$, $\gamma = 0.1$; parameter study of the number of sections; 100 cells.

$$m = n\frac{4}{3}\rho_l \pi \left(\frac{d}{2}\right)^3. \tag{37}$$

Extending model (34)–(36) to droplets of size d' before and d after splashing yields

$$v = -\alpha v', \quad d = \beta d', \quad m = (1-\gamma)m'. \tag{38}$$

Relation $(38)_{2,3}$ and (37) can be used to obtain the splashing condition

$$n = \frac{1-\gamma}{\beta^3} n', \tag{39}$$

a relation between the number of droplets before and after splashing. Consequently, droplets of diameter d' (or surface s') and velocity v' are splashed into $\frac{1-\gamma}{\beta^3}$ droplets of diameter $\beta d'$ (or surface $\beta^2 s'$) and velocity $-\alpha v'$.

Denoting the number of incident droplets of surface between s' and $s' + ds'$ and velocity between v' and $v' + dv'$ by $f^+(v', s')dv'ds'$ and those that are reflected by $f^r(v,s)dvds$, relation (39) can be transformed into the splashing condition

$$\begin{aligned} f^r(v,s)dvds &= \frac{1-\gamma}{\beta^3} f^+(v', s')dv'ds', \\ v &= -\alpha v', \quad s = \beta^2 s'. \end{aligned} \tag{40}$$

Eq. $(40)_2$ and $(40)_3$ can be used to transform $(40)_1$ into

$$f^r(v,s)dvds = -\frac{1-\gamma}{\alpha\beta^5} f^+\left(-\frac{v}{\alpha}, \frac{s}{\beta^2}\right) dvds. \tag{41}$$

Using this expression for all droplet sizes, it is tacitly assumed that the splashing of all droplets can be described with the same parameters α, β and γ. This simple model was chosen for clarity reasons but more advanced splashing models can be found, for example in Garcia Rosa et al. (2006) or Cossali et al. (2005). These more realistic models lead to splashing parameters that depend on the velocity and size of incident particles. Moreover, splashing depends directly on the conditions on or in the vicinity of the wall (cf. Rioboo et al., 2002). In the case of a dry wall, at least the wall temperature and the wall roughness are of relevance. If a liquid film forms on top of the wall which is usually changing in thickness, the mechanism of the splashing are completely changed (cf. Roisman and Tropea, 2002). The considerations of these influences on the splashing is not intended in this work, because with more refined splashing models, which in fact is a three-dimensional process, the one-dimensional model (3) cannot be improved anyway. Nevertheless, it has to be remarked that in a three-dimensional setting, the splashing parameters would describe the behaviour of the droplets close to the wall. The heavy interaction between incident and splashed droplets away from the wall (cf. Kyriopoulos et al., 2008) can be captured by collision, coalescence and breakup models, which are part of the general kinetic spray Eq. (1).

With relation (41) it is possible to compute the moments after splashing, $M^{(k)r}_{K,L}$, from the moments, $M^{(k)+}_{K,L}$, and parameters $\left\{a^1_{(k)}, U^1_{(k)}, a^2_{(k)}, U^2_{(k)}\right\}$ before splashing for all sections $k = 1, \ldots, N$.

To give an example of the exact relation between moments and parameters before and after splashing the derivation for $M^{(k)r}_{0,0}$ is illustrated. First, expression (41) is substituted into the definition of $M^{(k)r}_{0,0}$ (see (9)) which yields

$$M^{(k)r}_{0,0} = \int_{s_i}^{s_{i+1}} \int_{-\infty}^{\infty} \frac{1-\gamma}{\alpha\beta^5} f^+\left(-\frac{v}{\alpha}, \frac{s}{\beta^2}\right) dvds. \tag{42}$$

(42) is then transformed by a change of variables into the integral

$$M_{0,0}^{(k)r} = \int_{s_i/\beta^2}^{s_{i+1}/\beta^2} \int_{-\infty}^{\infty} \frac{1-\gamma}{\beta^3} f^+(u,t)\,du\,dt, \quad \text{with} \quad u = -\frac{v}{\alpha} \quad \text{and} \quad t = \frac{s}{\beta^2}. \tag{43}$$

It is important to note that in expression (43) the interval $[s_i/\beta^2, s_{i+1}/\beta^2[$ does not necessarily agree with the fixed sections chosen for the incident spray. Therefore, the moments related to the reflected droplets have to be computed from moments and parameters of more than one section.

It should also be noted that in this model the splashing is assumed to take place instantaneously, i.e. no special time or length scale is introduced for the splashing process.

It may also be of interest that, from the numerical point of view, the splashing condition has the character of both an outlet and an inlet condition applied at the same position in real space.

The procedure to compute the splashing at the right wall is structured in the following way:

(1) From the quadrature parameters in the cell next to the wall the approximate NDF of the incident droplets, $\tilde{f}^+$, is computed according to

$$\tilde{f}^+(u,t) = \sum_{j=1}^{2} \left\{ a^+_{(k)j}\,\delta(u - U^j_{(k)}) \right\} \exp(-b_k t) \tag{44}$$

where the parameters follow from

$$\begin{cases} a^+_{k,j} = a^j_k & \text{if } U^j_{(k)} \text{ positive,} \\ a^+_{k,j} = 0 & \text{otherwise.} \end{cases} \tag{45}$$

They are saved in a ghost cell on the right side of the wall.

(2) The moments of the reflected droplets $M^{(k)r}_{K,L}$ and the quadrature parameters are computed with relations like (43) and also saved in the ghost cell.

(3) The fluxes over the left boundary of the ghost cell are computed from the moments and quadrature parameters of the reflected droplets.

Fig. 1 depicts the steady state solutions of the number of droplets in a section, $M^{(k)}_{0,0}(s)$ (called 'droplet distribution') obtained for $\{5, 10, 20\}$ sections. They are compared with the Lagrangian calculations for the parameter set $(\alpha,\beta,\gamma) = (0.9, 0.7, 0.1)$. The number of cells is not varied because the spray is freely transported in the computational domain. Only at the boundary is the spray distribution changed. The high peak on the left side represents the splashed spray and is moving away from the wall (see averaged velocity distribution in Fig. 2), whereas the smaller peak on the right, agreeing with the inlet distribution (dashed line), is moving towards the wall. It is observed that for this test case the Lagrangian and Eulerian solutions for 10 and 20 sections are very close to each other. Reduction of the number of sections to five results in some discrepancies, but the qualitative behaviour of the moment method persists. The sensitivity of the method was studied for the change of parameters (α,β,γ). In Figs. 2–4 the droplet distributions are plotted versus the droplet surface at positions $x = 0.9$ for the sets of parameters $(\alpha,\beta,\gamma) = \{(0.5, 0.7, 0.1), (0.9, 0.5, 0.1), (0.9, 0.7, 0.5)\}$. Each set of parameter is compared with its Lagrangian solution and with the solutions shown in Fig. 1. In the lower plot of Fig. 2 the distribution of averaged droplet velocity, $M^{(k)}_{3/2,1}/M^{(k)}_{3/2,0}$, is also shown.

Fig. 2 illustrates what happens when droplets are reflected inelastically on a wall. The reduction of the absolute velocity value (lower part of Fig. 2) on the wall leads to an increase in the number density of the splashed droplets (upper part of Fig. 2), an obvious consequence of the mass conservation. The comparison between Lagrangian and Eulerian calculations shows good agreement for this deceleration effect and also the average velocities agree with those expected from the model in (34).

The breakage of the droplets is determined by the parameter β. Smaller values of this quantity result in more but smaller daughter droplets after splashing. This behaviour is shown in Fig. 3 for the Lagrangian and the Eulerian calculations.

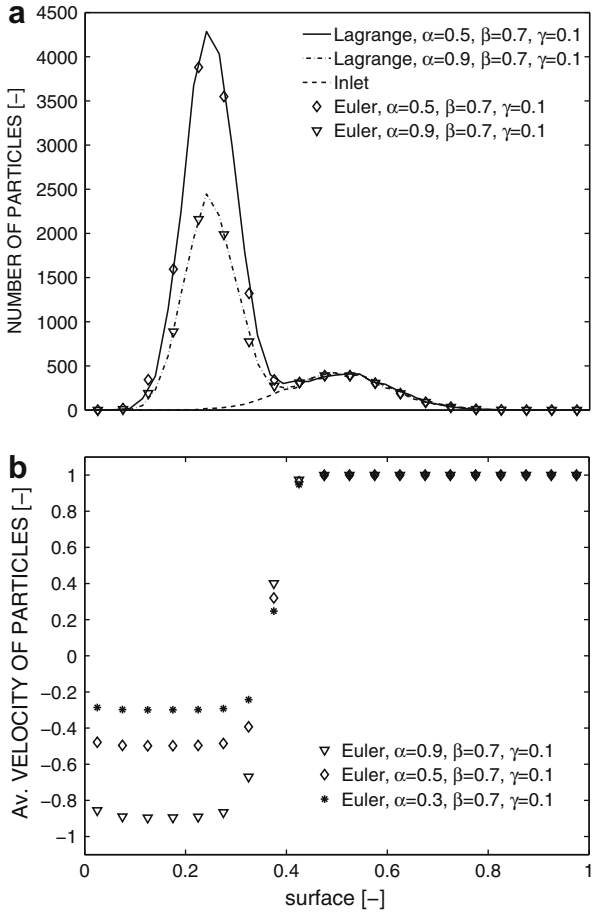

Fig. 2. Droplet distribution (upper), distribution of averaged droplet velocity (lower); splashing with parameters $(\alpha,\beta,\gamma) = \{(0.5, 0.7, 0.1)\}$ and $(\alpha,\beta,\gamma) = (0.9, 0.7, 0.1)$; 20 sections and 100 cells; position $x = 0.9$.

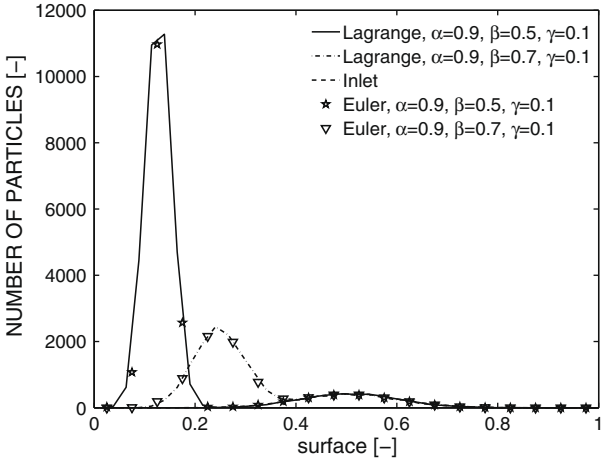

Fig. 3. Droplet distribution; splashing with parameters $(\alpha,\beta,\gamma) = (0.9, 0.5, 0.1)$ and $(\alpha,\beta,\gamma) = (0.9, 0.7, 0.1)$; 20 sections and 100 cells; position $x = 0.9$.

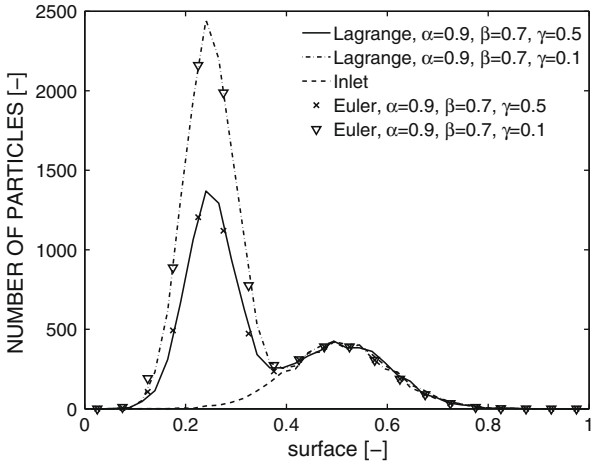

Fig. 4. Droplet distribution; splashing with parameters $(\alpha, \beta, \gamma) = (0.9, 0.7, 0.5)$ and $(\alpha, \beta, \gamma) = (0.9, 0.7, 0.1)$; 20 sections and 100 cells; position $x = 0.9$.

The model in (40) also includes a parameter, γ, that allows the consideration of mass deposition on the wall or sudden liquid evaporation due to a hot wall. For large values of γ a large amount of liquid mass is taken from the system. In Fig. 4 Lagrangian and Eulerian calculations are compared for two different values of γ. The Eulerian results recover the accurate Lagrangian solutions nicely.

6.2. Test case: crossing and evaporating spray

The phenomenon of droplet evaporation is dealt with in a vast amount of literature on single droplets or sprays (for an overview see Sirignano, 1999). For sprays, Laurent and Massot (2001), Laurent et al. (2004), Dufour and Villedieu (2005) and Schneider et al. (2008) have shown that the sectional method can capture evaporation very accurately with general evaporation models. However, for a configuration where two evaporating spray distributions are crossing each other, the sectional method as well as all other Eulerian methods for the prediction of sprays, fail to predict at least qualitatively the correct solution of the kinetic spray equation.

The method presented in Sections 3–5 is tested in a configuration in which two truncated Gaussian spray distributions (see inlet in Fig. 5) with different initial velocities $(v_L = 1,\ v_R = -2/3)$ at $x = 0$ and $x = 1$ are transported in real space, $x \in [0, 1]$, towards each other. The two initial spray distributions evaporate according to the d^2-law, i.e. they are shifted towards $s = 0$ (see (46)). In this model, the droplet drag force as well as heating, breakage and collision of droplets arising in (3) are assumed to be absent. With these assumptions the spray Eq. (3) reduces to

$$\frac{\partial(f)}{\partial t} + \frac{\partial(vf)}{\partial x} - \mathrm{Ev}\frac{\partial(f)}{\partial s} = 0. \tag{46}$$

In Fig. 5 the droplet distributions $(M^{(k)}_{0,0}(s))$ are shown for steady calculations of the moment method with $\mathrm{ns} = \{5, 10, 20\}$ sections and $\mathrm{nx} = \{50, 100, 200\}$ cells at positions $x = 0.5$ and $x = 0.9$. In addition, the inlet distributions (dashed lines) are depicted as well as the Lagrangian solutions (solid lines) which are regarded as accurate reference solutions. In the upper plot of Fig. 5 the two distributions have evaporated and overlap. This behaviour indicates that the distributions are crossing each other. If the method could not predict this behaviour, a delta shock would have formed at the point where the distributions first cross ($x = 0.6$). This shock would have moved according to the relation between the momenta of droplets in each section. All droplets that arrive at the delta shock would have concentrated there and, as the velocity of the left

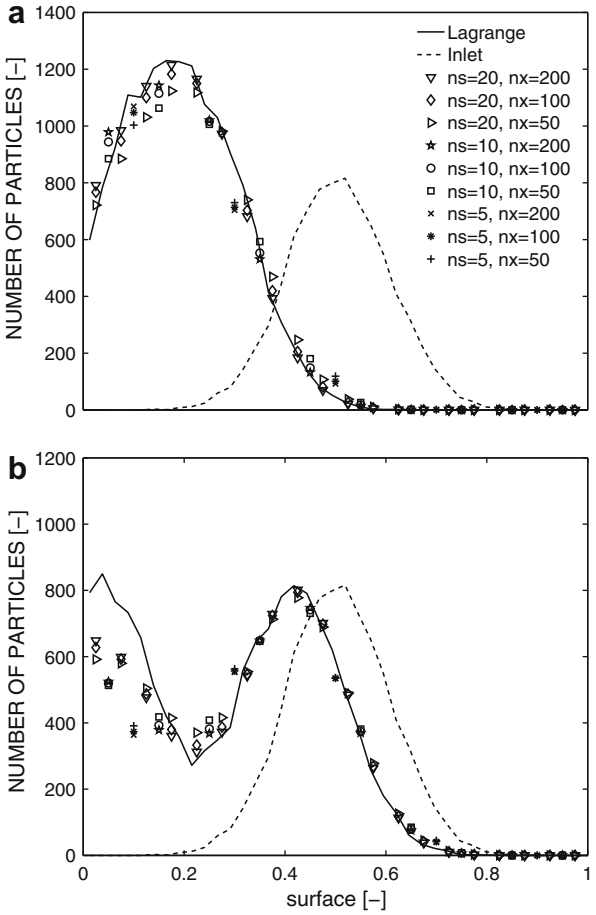

Fig. 5. Droplet distribution at $x = 0.5$ (upper) and $x = 0.9$ (lower); evaporation and crossing of spray jets with $\mathrm{Ev} = 0.52$; parameter study of the number of sections and cells.

distribution is larger, no droplet coming from the right of the computational domain could have reached $x = 0.5$. Indeed, the lower plot in Fig. 5 confirms the proposition that the two jets cross each other. The left peak represents the droplets coming from the left of the computational domain whereas the right peak originates from the right and has evaporated only slightly. As droplets coming from the left are existing at position $x = 0.9$, they must have crossed the spray distribution coming from the right.

Calculations with five sections are very crude but can still capture the evaporation and crossing effect of the spray. Using a larger number of sections improves the results considerably but still, as shown in the lower plot of Fig. 5, there is a discrepancy between the Lagrangian and Eulerian calculations. This defect of the moment method may originate from either numerical diffusion in surface space or follow from small numerical interactions between the two distributions crossing each other in the middle of the computational domain. The analysis of this behaviour and the improvement of the numerical procedures will be carried out in future study. The parameter study of the discretisation in real space gives the expected result. With smaller cell sizes the differences between Eulerian and Lagrangian calculations reduce.

By changing the values for Ev the sensitivity of the numerical method was tested. The droplet distributions at positions $x = 0.5$ and $x = 0.9$ are depicted in Fig. 6 for 10 sections and 100 cells. For smaller evaporation numbers the droplets are evaporated more slowly and remain longer in the computational domain. These tests show no correlation between accuracy of the Eulerian method and evaporation number.

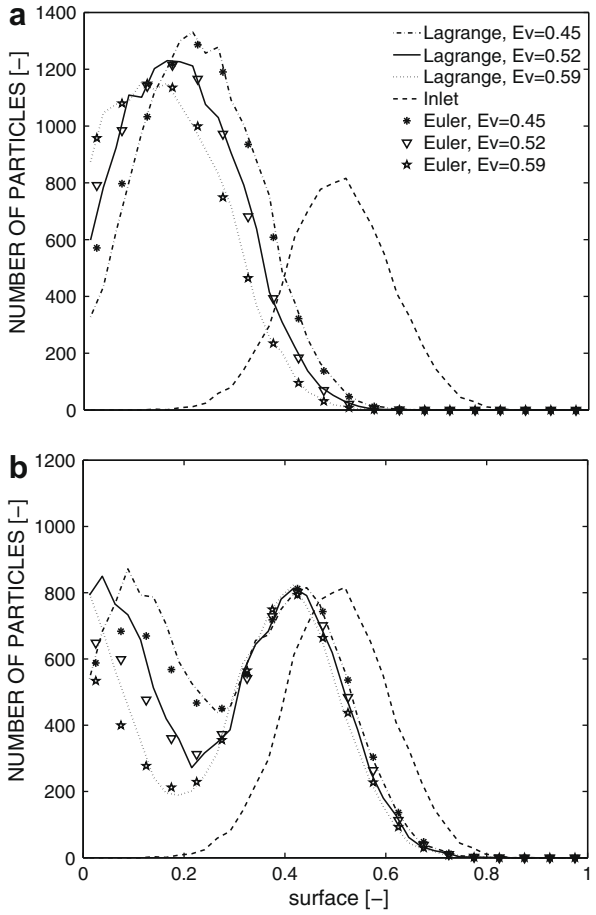

Fig. 6. Droplet distribution at $x = 0.5$ (upper) and $x = 0.9$ (lower); evaporation and crossing of spray jets; different evaporation numbers; 20 sections, 200 cells.

6.3. Test case: crossing sprays affected by drag

It was shown by Laurent and Massot (2001), Laurent et al. (2004), Dufour and Villedieu (2005) and Schneider et al. (2008) that the sectional method can accurately predict the behaviour of a spray which is affected by drag and gravity forces. In a polydisperse spray which is accelerated (or decelerated) by the surrounding gas, the forces on the droplets, and consequently their velocities, are correlated, among other things, with the size of a droplet.[5]

For the sectional method, droplets collected in one section exhibit the same velocities. Therefore, it is expected that the more sections come into play for the discretisation of size space the more accurate the dependence of the velocity on the size that is modelled with the sectional method. It is shown in this test case that the combination of the sectional method with the quadrature-based moment method from Desjardins et al. (2008) does not change the ability of the method to capture the phenomenon of drag affecting a spray.

In this test configuration two truncated Gaussian spray distributions are moving towards each other starting at the ends of the computational domain, $x \in [0, 1]$. During the crossing process, they are affected by a Stokes drag force which results from the velocity difference between the spray and a non-moving gas. This drag test case can never reach a steady state, because those droplets that are stopped by the gas before leaving the computational domain accumulate at a certain position until the computation stops. Smaller droplets decelerate faster and stop closer to where they come from. This phenomenon is commonly called size segregation of droplets.

In Fig. 7 the Eulerian results of the drag test case are depicted and compared to the calculations using a 'reference' Lagrangian method. The number of sections and cells are varied according to $\mathrm{ns} = \{5, 10, 20\}$ and $\mathrm{nx} = \{50, 100, 200\}$, respectively and the upper, middle and lower plot refer to the results at positions $x = 0.5$, $x = 0.7$ and $x = 0.9$, respectively.

For all results shown in the three plots in Fig. 7, the droplet distributions are much higher than the initial distribution. The reason

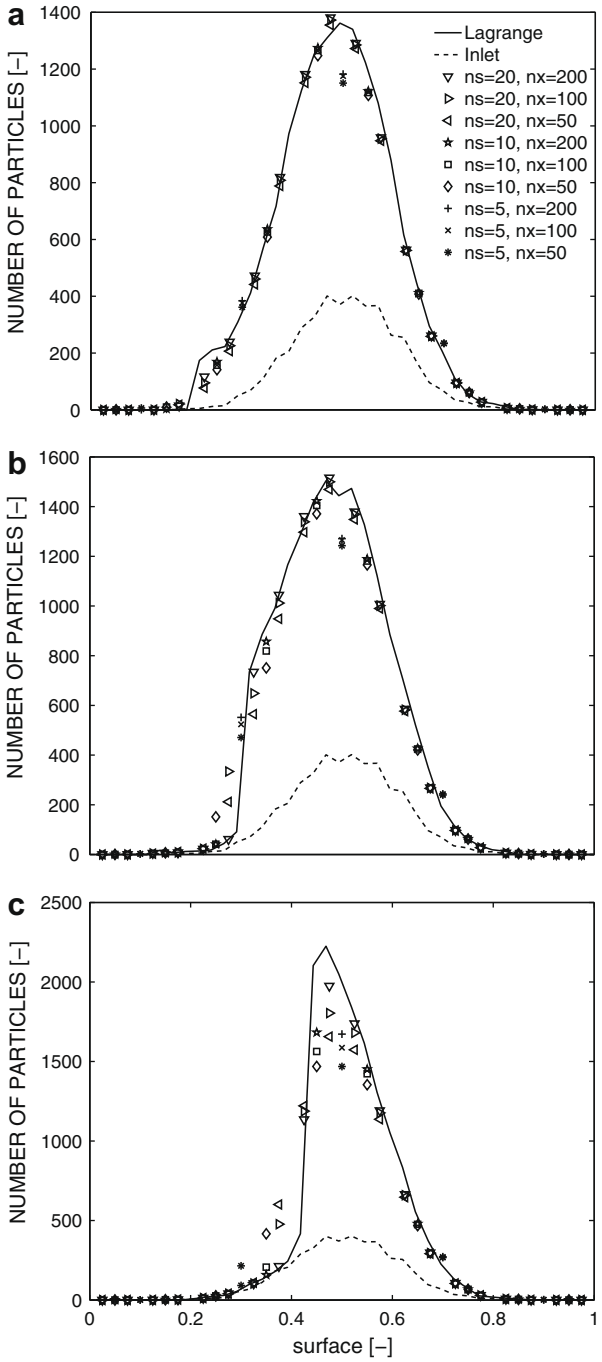

Fig. 7. Droplet distribution at $x = 0.5$ (upper), $x = 0.7$ (middle) and $x = 0.9$ (lower); crossing sprays affected by Stokes drag with $\mathrm{St}_{max} = 2.43$; parameter study of the number of sections and cells.

[5] In general, the acceleration (or deceleration) of a droplet is not only determined by its size but also by its mass density, its shape and its dynamic behaviour. In the Stokes drag model in (2) only differences in size and mass density result in different droplet accelerations. Here, the droplets are assumed to have the same mass density.

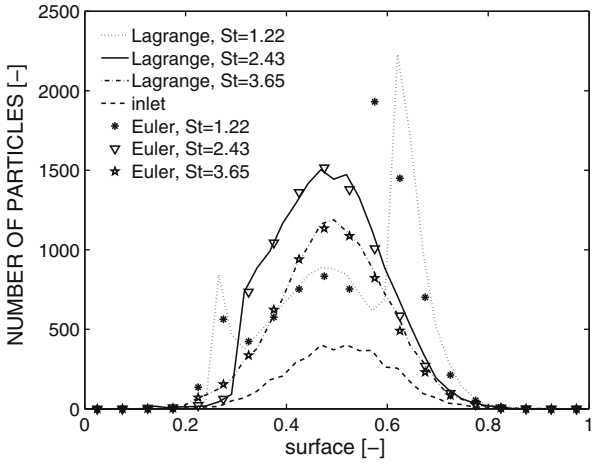

Fig. 8. Droplet distribution at $x = 0.7$; crossing sprays affected by Stokes drag; parameter study for different Stokes numbers; 20 sections, 200 cells.

for this behaviour is, first, the deceleration of droplets which leads to an accumulation and secondly, the overlap of the crossing distributions.

It is also observed that all graphs in Fig. 7 exhibit an asymmetry in the distribution. This effect is due to the drag force. Small droplets on the left sides of the graphs experience a strong deceleration and stop before they leave the computational domain. The steep gradient, observed in all graphs, marks the border between stopped droplets (left side of the steep gradient) and moving droplets (right side of the steep gradient). In the plot for $x = 0.9$, on the left side of the steep gradient, there are droplets which have not stopped and which agree very well with the droplet distribution of the inlet distribution. Those droplets belong to the distribution coming from the right.

The parameter study of the moment method for the number of sections and cells shows the expected results. Increasing the discretization in size and real space decreases the difference between the Lagrangian and Eulerian predictions.

In the plot for $x = 0.9$ the improvement due to the increase from 50 to 200 cells is very pronounced. This behaviour can be explained by the fact that the increase of maximum droplet density between $x = 0.5$ and $x = 0.7$ is much smaller than between $x = 0.7$ and $x = 0.9$. This strong gradient of the droplet density in real space requires a finer x-discretisation in order to obtain a more accurate solution. For the variation of the number of sections it is observed that there is only a small difference between solutions using 10 and 20 sections. With five sections the qualitative behaviour of the drag effect can be captured.

The Stokes number of the largest droplets, St_{max}, is varied according to $\mathrm{St}_{max} = \{1.22, 2.43, 3.64\}$ to test the sensitivity of the method. In Fig. 8 the Eulerian solutions with 20 sections and 200 cells are compared with the Lagrangian results at position $x = 0.7$. For the smallest St_{max} the concentration of droplets is very pronounced for both, the distribution moving to the left (left peak) and the distribution moving to the right (right peak). It is also observed that the gradients in size and real space are the steepest. This behaviour is due to the strong deceleration and standstill of the droplets. The Eulerian results can predict the left peak very well but the right peak is not captured correctly. The reason may be a discretisation of the size and velocity space which is not fine enough. For larger St_{max} the Lagrangian results are recovered very well.

7. Conclusions

It is demonstrated in a one dimensional setting that the new moment method can describe polydisperse sprays that splash on a wall and that cross each other while they are evaporating or experiencing a Stokes drag force. So far, Eulerian methods, like that of Gelbard et al. (1980), Domelevo (2001), Laurent and Massot (2001), Laurent et al. (2004) or Dufour and Villedieu (2005) were only able to describe the dispersion with respect to the size variable, then being able to capture accurately evaporation, coalescence and drag of a polydisperse spray. On the other hand, Desjardins et al. (2008) took into account the dispersion with respect to the velocity variable, allowing the description of crossing and splashing monodisperse sprays. The moment method derived and tested here considers both variables and is therefore able to predict all combinations of polydisperse and crossing effects of sprays.

In the cases of splashing and drag, the comparison of the new moment method with accurate Lagrangian calculations reveals a convincing agreement even for small numbers of sections. The results for splashing and drag in Section 6 indicate that 5–10 sections are enough to describe polydisperse effects. Using more sections, the issue of computational costs arises in the application of the new method, particularly when it is extended to higher dimensions in real space. For the evaporation test case, the discretisation of the size space with a small number of sections leads to qualitative, correct results but unfortunately some discrepancies between Eulerian and Lagrangian calculations are observed. This behaviour requires further study to improve the numerical procedures for the evaporation part of the method.

A new but academic splashing model was proposed and adapted to the moment method in Section 6. It is indicated how this simple model can be extended to realistic splashing configurations. However, the heavy interaction between the incident and splashed droplets away from the wall requires the consideration of coalescence and breakup. These phenomenon have not yet been tested with this method, but their consideration is, in principle, possible. Laurent et al. (2004) have studied coalescence and breakup using the sectional method.

Obviously, the new moment method still awaits the extension to higher dimensions in real space and finer discretisation of the velocity space (see parameter I in (11)). Its ability to capture the polydisperse nature of sprays as well as the coexistence of two $(I = 2)$ droplet velocities at one location is clearly demonstrated. Despite the strong assumptions made in this work, it opens a new way of describing unsteady spray phenomena with Eulerian methods.

Acknowledgement

The first author acknowledges the financial support received via the Technical University of Darmstadt from 2006 to 2008.

References

Abramzon, B., Sirignano, W., 1989. Droplet vaporization model for spray combustion calculations. Int. J. Heat Mass Transfer 32, 1605–1618.
Bobylev, A.V., Ohwada, T., 2001. The error of the splitting scheme for solving evolutionary equations. Appl. Math. Lett. 14, 45–58.
Boileau, M., Staffelbach, G., Cuenot, B., Poinsot, T., Bérat, C., 2008. LES of an ignition sequence in a gas turbine engine. Combust. Flame 154, 2–22.
Boltzmann, L., 1898. Vorlesungen zur Gastheorie (Lectures on Gas Theory). Ambrosius Barth, Leipzig, Reprint: Boltzmann, L., 1995. Lectures on Gas Theory. Dover Publications Inc.
Borée, J., Ishima, T., Flour, I., 2001. The effect of mass loading and inter-particle collisions on the development of the polydispersed two-phase flow downstream of a confined bluff body. J. Fluid Mech. 443, 129165.
Bouchut, F., 1994. On zero pressure gas dynamics. In: Perthame, B. (Ed.), Advances in kinetic theory and computing, Series Advances in Mathematics for Applied Sciences, vol. 22. World Scientific, River Edge, NJ, pp. 171–190.
Cercignani, C., 1988. The Boltzmann Equation and its Applications. Springer, New York, Berlin, etc..
Cossali, G.E., Marengo, M., Santini, M., 2005. Single-drop empirical models for spray impact on solid walls: a review. Atomization Sprays 15, 699–736.

Costa, C.B.B., Maciel, M.R.W., Filho, R.M., 2006. Considerations on the crystallization modeling: population balance solution. Comput. Chem. Eng. 31, 206–218.
Crowe, C., Sommerfeld, M., Tsuji, Y., 1998. Multiphase Flows with Droplets and Particles. CRC Press.
Desjardins, O., Fox, R.O., Villedieu, P., 2008. A quadrature-based moment method for dilute fluid-particle flows. J. Comput. Phys. 227, 2514–2539.
Domelevo, K., 2001. The kinetic-sectional approach for noncolliding evaporating sprays. Atomization Sprays 11, 291–303.
Drew, D.A., Passman, S.L., 1999. Theory of multicomponent fluids. Applied Mathematical Sciences, vol. 135. Springer, New York, Berlin, etc..
Dufour, G., Villedieu, P., 2005. The sectional method revisited for evaporating sprays. M2AN Math. Model. Numer. Anal. 39, 931–936.
Dukowicz, J.K., 1980. A particle-fluid numerical model for liquid sprays. J. Comput. Phys. 35, 229–253.
Février, P., Simonin, O., Squires, K.D., 2005. Partitioning of particle velocities in gas–solid turbulent flows into a continuous field and a spatially uncorrelated random distribution: theoretical formalism and numerical study. J. Fluid Mech. 533, 146.
Fox, R.O., 2008. A quadrature-based third-order moment method for dilute gas-particle flows. J. Comput. Phys. 227, 6313–6350.
Fox, R.O., Laurent, F., Massot, M., 2008. Numerical simulation of spray coalescence in an Eulerian framework: direct quadrature method of moments and multi-fluid method. J. Comput. Phys. 227, 3058–3088.
Garcia Rosa, N.G., Villedieu, P., Dewitte, J., Lavergne, G., 2006. A new droplet-wall interaction model. In: 10th International Congress on Liquid Atomization and Spray Systems, ICLASS06-167.
Gelbard, F., Tambour, Y., Seinfeld, J.H., 1980. Sectional representations for simulating aerosol dynamics. J. Colloid Interface Sci. 76, 541–556.
Ghosal, S., Herrmann, M., 2006. Modeling sprays by the method of Laplace transforms. In: Proceedings of the 2006 Summer Program, Center for Turbulence Research, pp. 235–245.
Groll, R., 2002. Numerische Modellierung der Verdunstung turbulenter Zwei-Phasen-Strömungen mittels eines Euler/Euler-Verfahrens. Ph.D. Thesis, Technical University Darmstadt.
Grosch, R., Briesen, H., Marquardt, W., 2007. Generalization and numerical investigation of QMOM. AIChE J. 53, 207–227.
Ham, F., Apte, S.V., Iaccarino, G., Wu, X., Herrmann, M., Constantinescu, G., Mahesh, K., Moin, P., 2003. Unstructured LES of reacting multiphase flows in realistic gas turbine combustors. Technical Report, Center for Turbulence Research, Stanford.
Hutter, K., Jöhnk, K., 2004. Continuum Methods of Physical Modeling. Springer, New York, Berlin, etc..
Kaufmann, A., 2004. Towards Eulerian–Eulerian large eddy simulation of reactive two-phase flows. Ph.D. Thesis, Institute National Polytechnique de Toulouse.
Kyriopoulos, O., Roisman, I.V., Gambaryan-Roisman, T., Stephan, P., Tropea, C., 2008. Dynamics of a liquid film produced by spray impact onto a heated target. In: Proceedings of the 22nd European Conference on Liquid Atomization and Spray Systems, Como Lake, Italy.
Laurent, F., Massot, M., 2001. Multi-fluid modelling of laminar polydisperse spray flames: origin, assumptions and comparison of sectional and sampling methods. Combust. Theory Modell. 5, 537–572.
Laurent, F., Massot, M., Villedieu, P., 2004. Eulerian multi-fluid modeling for the numerical simulation of coalescence in polydisperse dense liquid sprays. J. Comput. Phys. 194, 505–543.
LeVeque, R.J., 1992. Numerical methods for conservation laws. Lectures in Mathematics, ETH Zurich, Birkhuser.
Marchisio, D.L., Fox, R.O., 2005. Solution of population balance equations using the direct quadrature method of moments. J. Aerosol Sci. 36, 43–73.
Merker, G.P., Schwarz, C., Stiesch, G., Otto, F., 2006. Simulating Combustion. Springer, New York, Berlin, etc..
O'Rourke, P.J., 1981. Collective drop effects on vaporizing liquid sprays. Ph.D. Thesis, Los Alamos National Laboratory.
Passman, S.L., Nunziato, J.W., Walsh, E.K., 1984. A theory of multiphase mixtures. In: Truesdell, C. (Ed.), Rational Thermodynamics, second ed. Springer, New York, Berlin, etc., pp. 286–325.
Pope, S.B., 2000. Turbulent Flows. Cambridge University Press.
Putnam, A., 1961. Integrable form of droplet drag coefficient. ARS J. 31, 1467.
Rhee, H.-K., Aris, R., Amundson, N.R., 2001. Theory and Application of Hyperbolic Systems of Quasilinear Equations: Theory and Application of Hyperbolic Systems of Quasilinear Equations. Dover Publications.
Riber, E., Moureau, V., Garcia, M., Poinsot, T., Simonin, O., 2009. Evaluation of numerical strategies for large eddy simulation of particulate two-phase recirculating flows. J. Comput. Phys. 228, 539–564.
Rioboo, R., Marengo, M., Tropea, C., 2002. Time evolution of liquid drop impact onto solid, dry surfaces. Exp. Fluids 33, 112–124.
Roisman, I.V., Tropea, C., 2002. Impact of a drop onto a wetted wall: description of crown formation and propagation. J. Fluid Mech. 472, 373–397.
Rueger, M., Hohmann, S., Sommerfeld, M., Kohnen, G., 2000. Euler/Lagrange calculations of turbulent sprays: the effect of droplet collisions and coalescence. Atomization Sprays 10, 47–81.
Schneider, L., Sadiki, A., Janicka, J., 2008. A study of the Eulerian multi-fluid method for an accelerating and evaporating spray. In: 22nd European Conference on Liquid Atomization and Spray Systems, pp. 2–8.
Sirignano, W.A., 1999. Fluid Dynamics and Transport of Droplets and Sprays. Cambridge University Press.
Strang, G., 1968. On the construction and comparison of difference schemes. SIAM J. Numer. Anal. 5, 506–517.
Vanni, M., 2000. Approximate population balance equations for aggregation–breakage processes. J. Colloid Interface Sci. 221, 143–160.
Williams, F.A., 1958. Spray combustion and atomization. Phys. Fluids 1, 541–545.